Supplementary Materials for

High-Resolution EM of Colloidal Nanocrystal Growth Using Graphene Liquid Cells

Jong Min Yuk, Jungwon Park, Peter Ercius, Kwanpyo Kim, Daniel J. Hellebusch, Michael F. Crommie, Jeong Yong Lee,† A. Zettl,† A. Paul Alivisatos†

†To whom correspondence should be addressed. E-mail: j.y.lee@kaist.ac.kr (J.Y.L.); azettl@berkeley.edu (A.Z.); alivis@berkeley.edu (A.P.A.)

Published 6 April 2012, *Science* **336**, 61 (2012)
DOI: 10.1126/science.1217654

This PDF file includes:

Other Supplementary Material for this manuscript includes the following:
(available at www.sciencemag.org/cgi/content/full/336/6077/61/DC1)

Movies S1 and S2

S1. Supporting Movie Legends

Movie S1. This movie shows diffusion and coalescence of nanocrystals. The frame rate is ~3.85/sec. Two movies were taken back-to-back with a dead time of 5 seconds between them; they were combined for Movie S1. The dead time is seen as a gap data in Fig. 3A.

Movie S2. This movie shows diffusion, oriented attachment, and faceting of nanocrystals. The frame rate is ~ 3.85/sec.

S2. Methods

Preparation of GLC sample. Growth dynamics of platinum nanocrystals in a graphene liquid cell was observed *in-situ* using a TEAM I. A growth solution of Pt(acetylacetonate)$_2$ (10 mg/mL) in a mixture of *o*-dichlorobenzene and oleylamine (9:1 in volume ratio) was used. The success rate in producing viable GLCs is >90%.

Pt growth in GLC. The growth of platinum nanocrystals was initiated by electron beam irradiation. Electron beam intensity was optimized onto local spots for the initial ~ 5 seconds of Movie S1 and S2 to capture the initial stage of nanocrystal growth. Liquid films for Movie S1 and S2 were thin enough to capture these initial stages. The electron beam intensity was maintained same throughout observation time and provided optimal contrast for nanocrystal motions. With thicker liquid films, contrast is very poor; however, liquid thickness can also be thinned by very strong electron beam irradiation (such conditions did not apply to the data shown here). Our TEM observations reveals that graphene secure liquid within pockets throughout the duration of the recording, usually ten to twenty minutes. ”

Microscopy. The low magnification TEM imaging was performed in a JEM-2010 LaB_6 instrument (JEOL Ltd.) at 100 kV.

High-resolution TEM images were acquired with the TEAM 1 operated at 80kV at the National Center for Electron Microscopy. This electron microscope has a high-brightness gun (X-FEG) and probe as well as image and chromatic aberration correctors. The image corrector (C_s) was fine tuned to obtain a third-order spherical aberration of −10μm, which in consideration of the positive fifth-order aberration (C_5) of 2.5 mm yielded optimal phase contrast with slight positive defocus. The theoretical information limit of 0.05 nm can thus be achieved at 80 kV. The resulting electron dose is approximately 4×10^5 e^-/sec·nm^2. We set 0.03 seconds of exposure time, 0.23 seconds of read out time, and therefore 0.26 seconds of entire frame time to acquire time-serial images. More details of the microscope configuration can be found elsewhere [32].

AFM images were taken on a MFP-3D scanning probe microscope (Asylum Research instruments). AFM imaging was performed on suspended GLC samples on Quantifoil TEM grids in non-contact mode using a V-shaped 'NSC35' probe C (phosphorus-doped Si with frequency f_c = 150 kHz, spring constants k = 4.5 N m^{-1}, and nominal tip radius 10 nm). All images were collected under ambient conditions at 23 °C with a scanning rate of 2.5-10 um/s.

SEM images were performed using FEI XL3000 at 5 kV.

Spectroscopy. The Raman measurements were performed using Renishaw inVia Raman microscope with 514 nm Ar ion laser.

S3. Text

Diffusivity of Pt nanocrystal. Two-dimensionally projected positions for a single nanocrystal trajectory are tracked in Movie S1 as it grows from 0.28 to 0.55 nm in radius by monomer attachment. As it grows, the particle diffusion slows as expected for Brownian motion (in the SiN cell the diffusivity does not scale this way due to substrate interactions). The trajectory is

divided into three equal parts based on time. As the nanocrystal grows with time, the mean square displacement (MSD) $\langle x^2 \rangle$ decreases (Fig. S8A). Representative TEM images of the nanocrystal at each time frame are displayed in Fig. S8B with color gradient mapped images for clarification. The two-dimensional diffusivity D is extracted from the slope of the MSD as a function of time; the corresponding nanocrystal size is averaged for each time regime. Figure S8C shows that the measured D of a nanocrystal decreases monotonically as the nanocrystal steadily grows. One similarity with previous tracking studies in the silicon nitride window cells is that the nanocrystal diffusivities in the confined liquid are found to be smaller than those expected from the bulk liquid viscosity (*26*).

Coalescence of Pt nanocrystals. We observed twenty coalescence events between NCs with diameters greater than 1 nm in Movie S2. We assume that coalescence events of NCs with smaller size or parallel to the electron beam cannot be distinguished or detected, respectively, and thus are not considered. One important factor to consider prior to discussing coalescence dynamics is NCs rotational degree of freedom. Figure S9 exhibits different lattice planes of a freely rotating NC at different times of observation. For this specific NC, lattice planes were observed eight times while the zone axis aligned with the beam over the course of the video; otherwise no fringes were observed off the crystal zone axes. Most coalescence we distinguished by lattice planes from Movie S2 occur along the along {111} planes of either one or both NCs, as represented in Fig. 2, Fig. S10, and Fig. S11. Only two coalescence events surveyed merged on different planes of the contacting NCs: {110} plane for one and off-zone axis for the other (Fig. S12).

The ratios of two NC diameters in Figs. 2B and 2C before coalescence are 0.75 and 0.71, respectively, which are similar with diameter ratios of two domains with twin boundaries after coalescence, 0.74 and 0.68 in Figs. 2B and 2C, respectively. Diameter is calculated using $D=2(A/\pi)^{0.5}$, where A is the projected 2D area of the NC in the video images. This consistency of

diameter ratio before and after coalescence is shown in all of NCs with twin boundaries in Movie S2 (Fig. S11).

S3. Supporting Figures and Legends

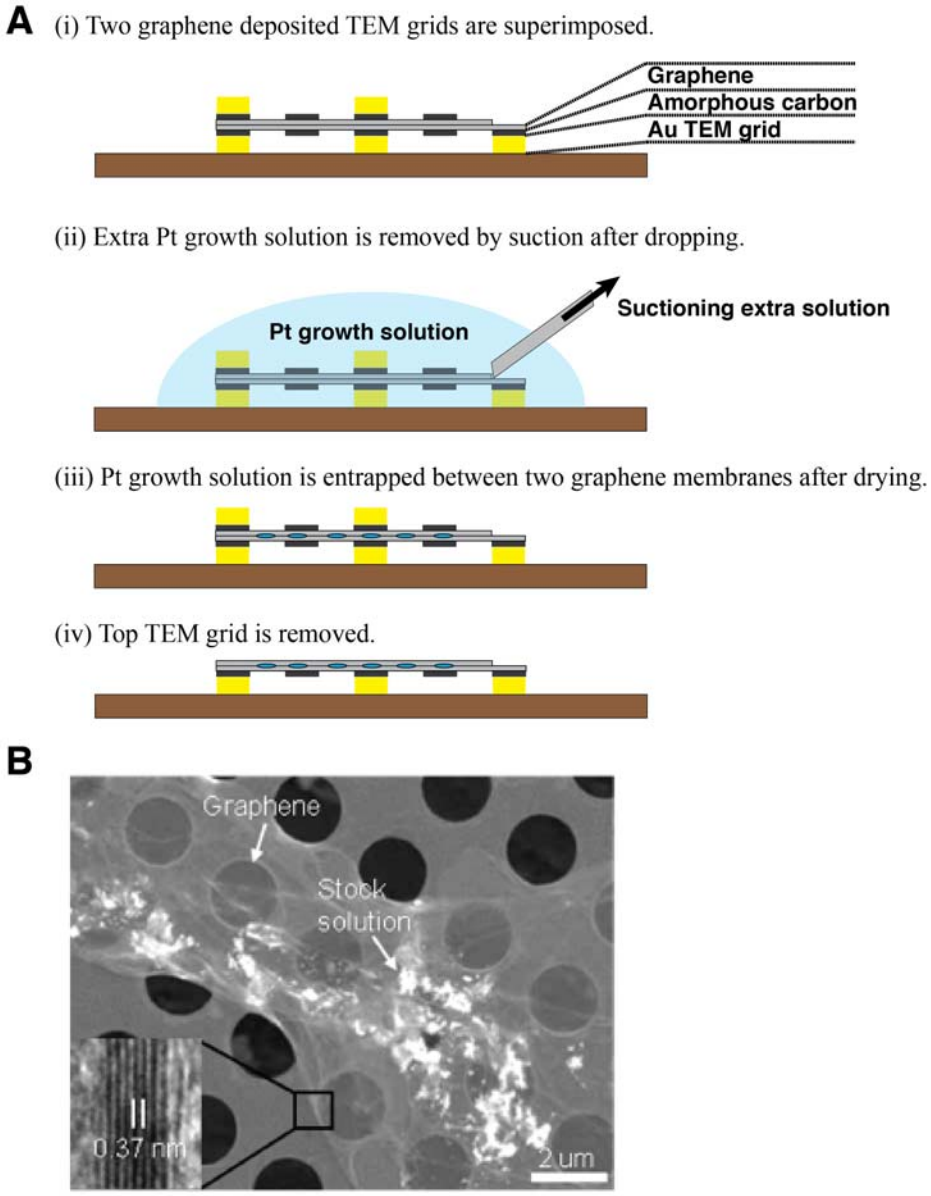

Fig. S1. Preparation of a graphene liquid cell. **(A)** Illustration of the fabrication processes of the graphene liquid cell. **(B)** SEM image of a graphene liquid cell. The inset is a TEM image of a nine-layered graphene on edge; that the distance between adjacent graphene layers is 0.37 nm.

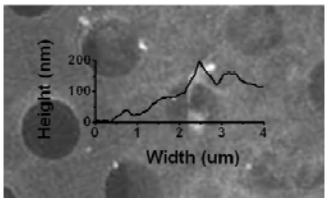

Fig. S2. AFM image and height profile of a GLC supported on a holey a-C grid. Encapsulated Pt growth solution appears white in the image and yields a spike in the height profile.

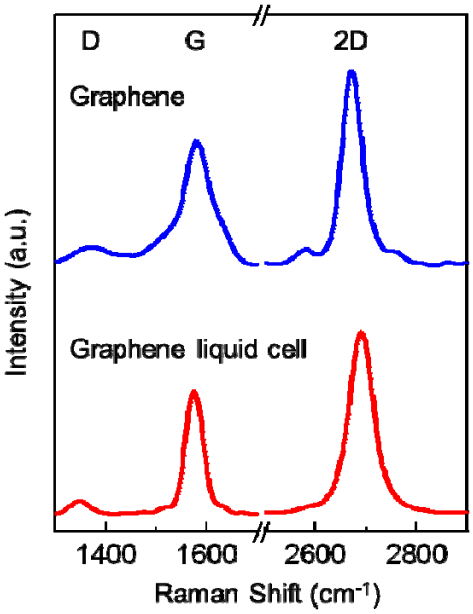

Fig. S3. Raman spectra of graphene deposited on TEM grid and graphene liquid cell.

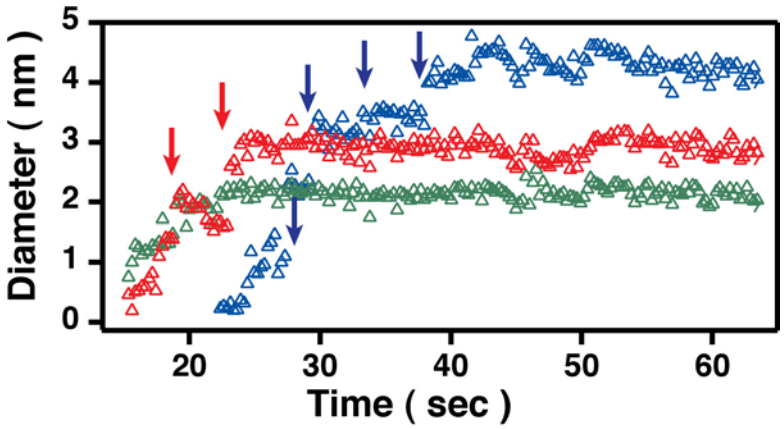

Fig. S4. Growth trajectories of individual Pt nanocrystal in several pathways: gradual growth by monomer addition, green; a single coalescence, red; and multiple coalescence, blue. Arrows indicate coalescence events.

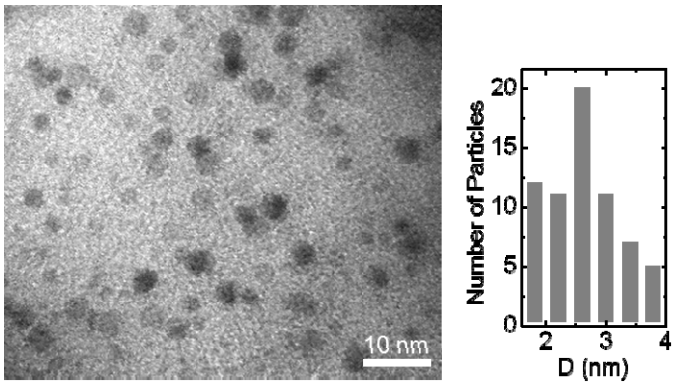

Fig. S5. Bright-field TEM image of Pt nanocrystals synthesized in a graphene liquid cell by the exposure of the growth solution to the electron beam for about 5 min and with corresponding particle diameter (D) histogram.

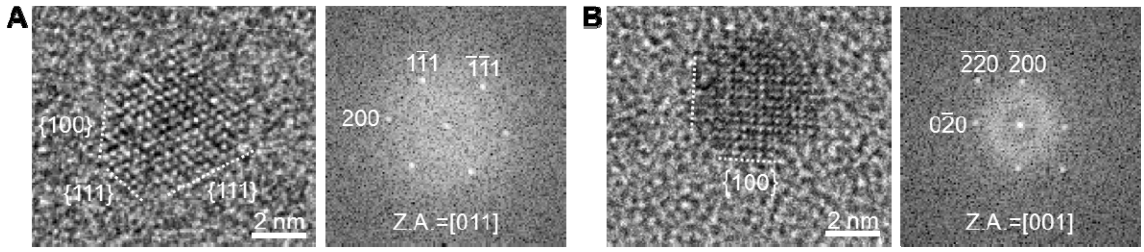

Fig. S6. High-resolution TEM images and FFT patterns of Pt nanocrystals **(A)** along the [011] zone axis (Z.A.) showing {100} and {111} facets and **(B)** along the [001] direction showing {100} facets.

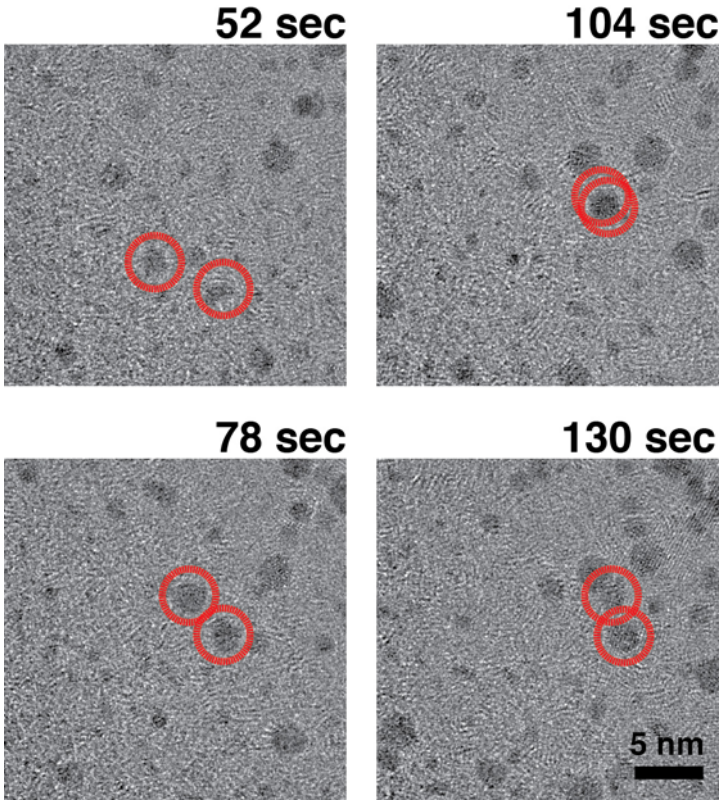

Fig. S7. Stil snapshots of two nanocrystals showing correlated motion before coalescence.

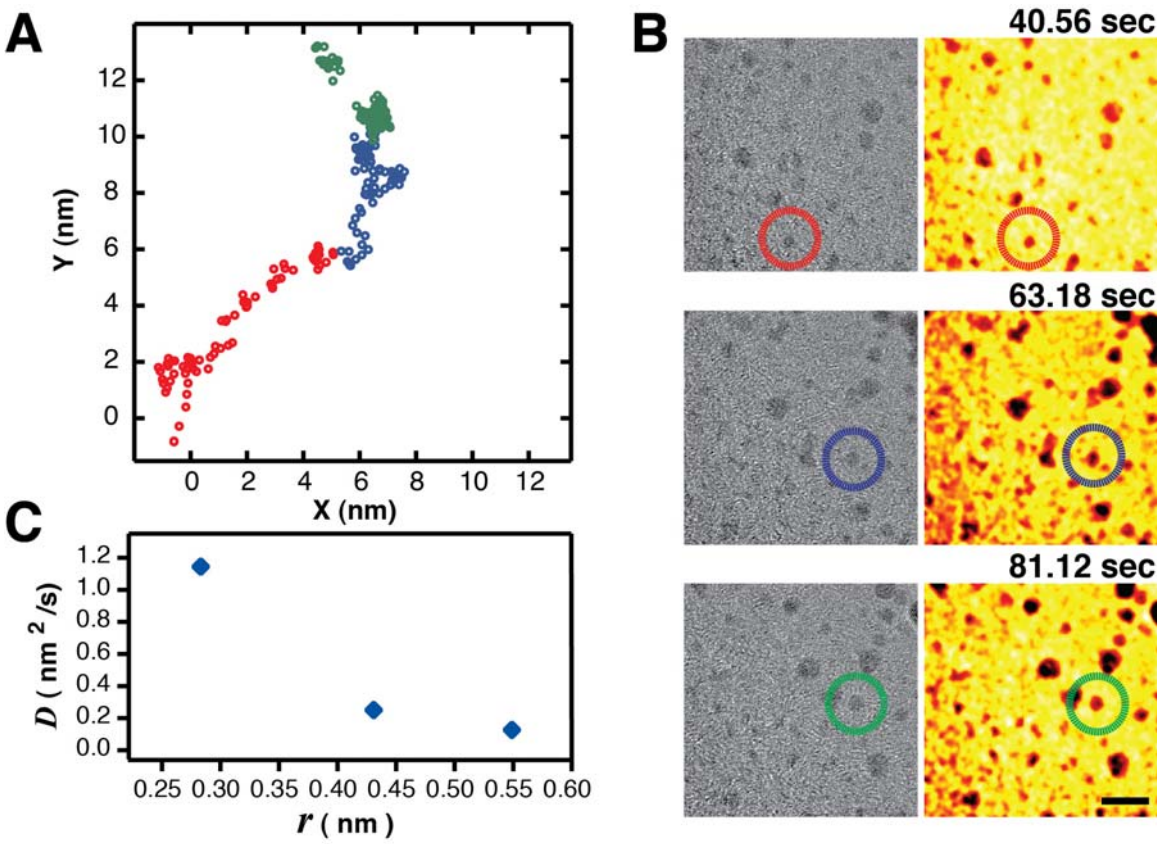

Fig. S8. Tracking of nanocrystal position and measured diffusivity with average size from 0.28 nm to 0.55 nm in radius during growth. **(A)** Positions of a nanocrystal in consecutive time regimes of 20 seconds each during growth: red, blue, and green colors indicate the earliest to final time regime, respectively. **(B)** Representative TEM images from Movie S1 of the tracked nanocrystal in the different time regimes. Colors of the circles match the time regimes in (A). The panels on the right are false-color representations of the TEM contrast data. Scale bars represent 5 nm. **(C)** Diffusivity *D* as a function of average nanocrystal radius (*r*) over the 20 seconds of each regime.

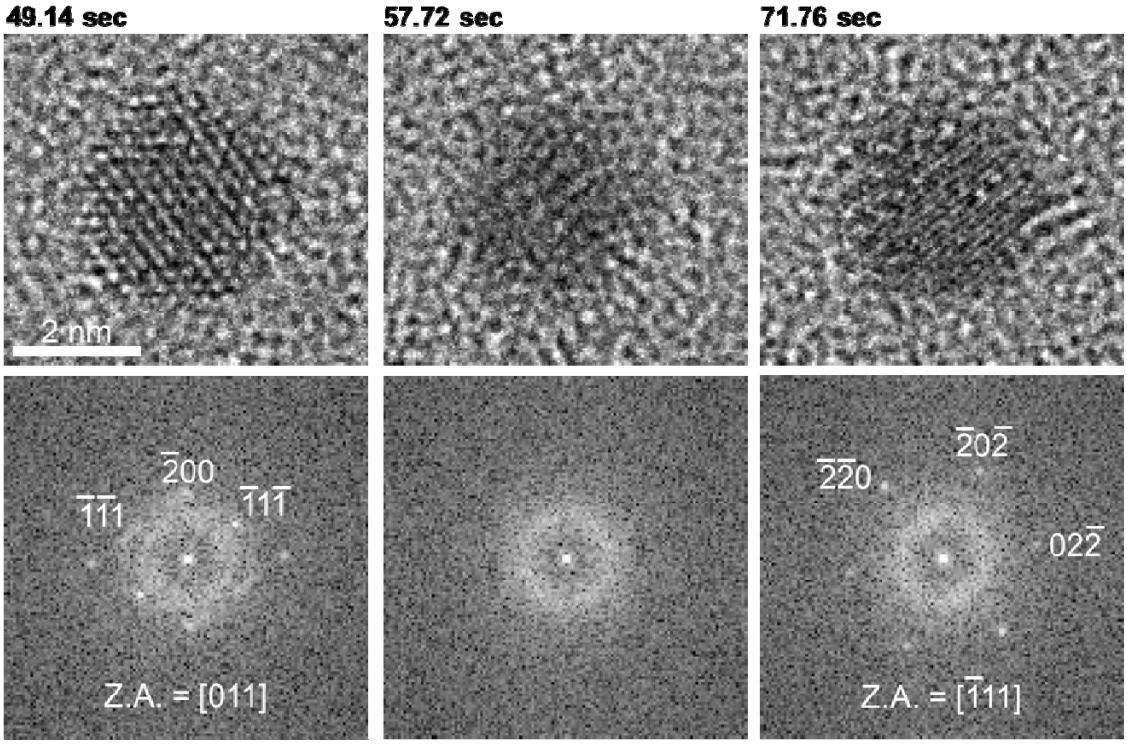

Fig. S9. From Movie S2, still snapshots and fast Fourier transformed (FFT) patterns showing free rotation of a nanocrystal in GLC. The nanocrystal is on [011] zone axis at 49.14 sec, rotates off zone axis at 57.72 sec, and has $[\bar{1}11]$ zone axis at 71.76 sec.

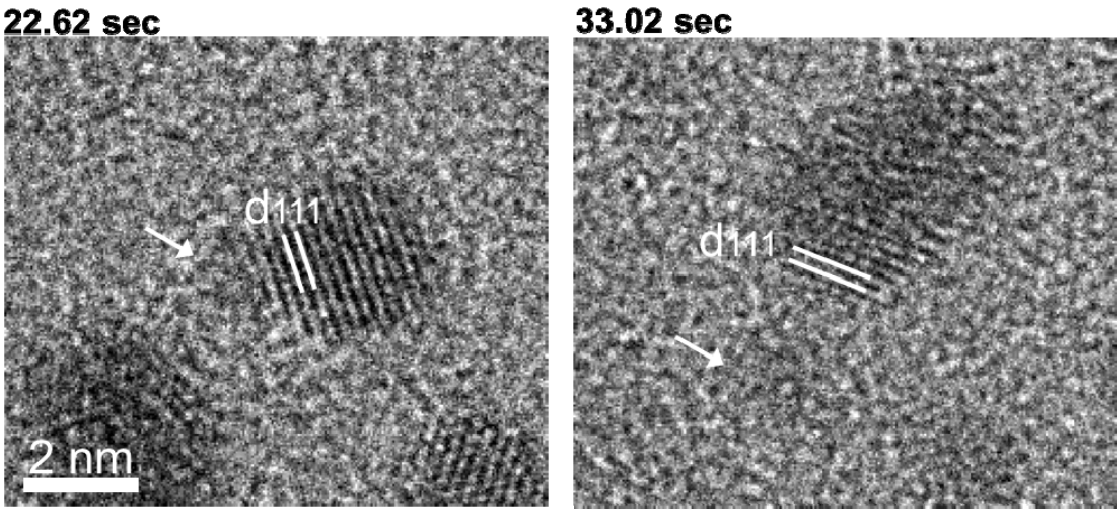

Fig. S10. From Movie S2, still snapshots showing coalescence of Pt nanocrystals on or near [011] zone axis. Coalescence evens happen at {111} planes in one of two nanocrystals at 22.62 and 33.02 sec. Incoming small nanocrystals indicated by arrows do not have any zone axes.

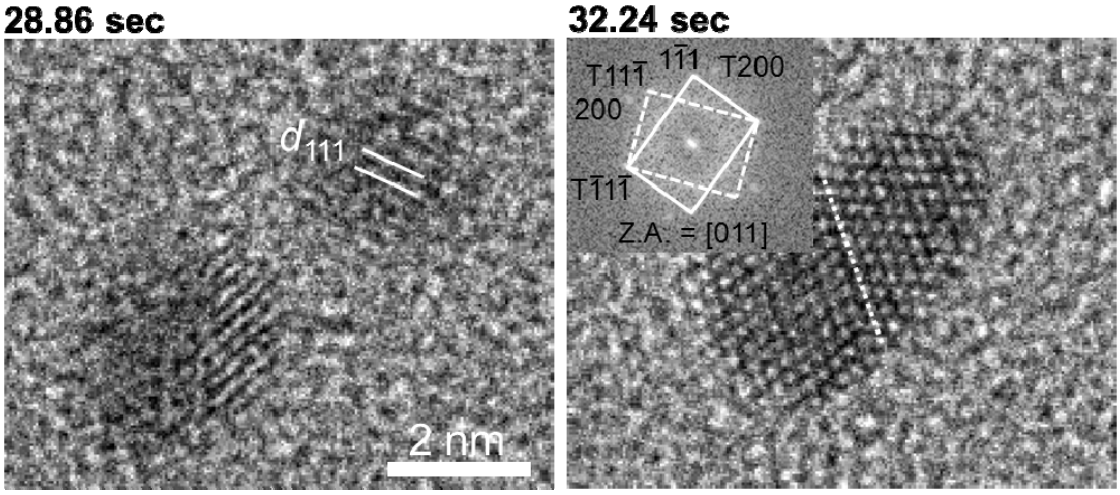

Fig. S11. From Movie S2, still snapshots showing the twin boundary in a merged nanocrystal after coalescence of nanocrystals on or near [011] zone axis. At 28.86 sec, the ratio of two nanocrystal diameters before coalescence is 0.88, which is similar with 0.86 of diameter ratio of two domains with twin boundary (dotted line) at 32.24 sec after coalescence.

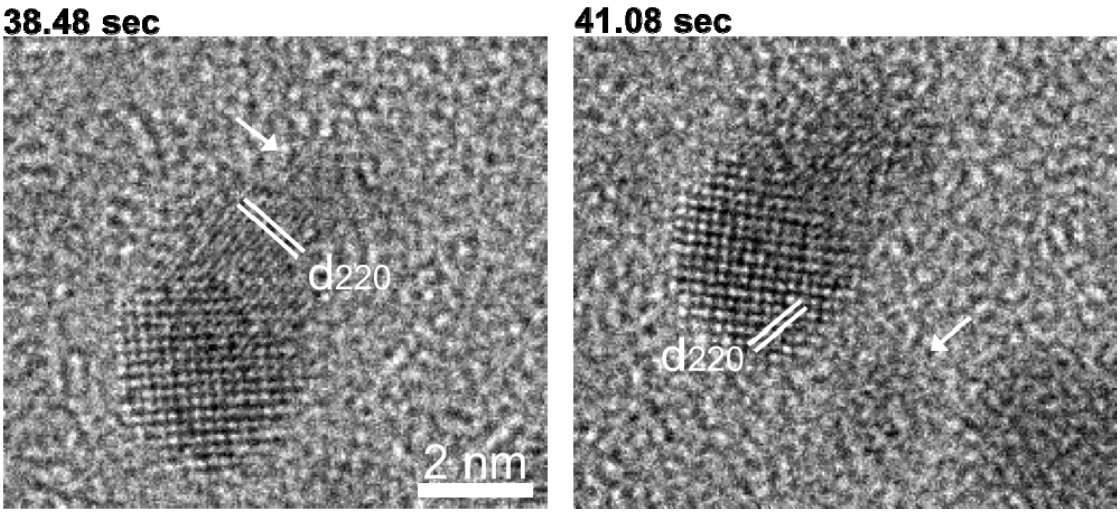

Fig. S12. From Movie S2, still snapshots showing coalescence of Pt nanocrystals on or near [001] zone axis. Coalescence evens happen at {110} planes in one of two nanocrystals at 38.48 and 41.08 sec. Incoming small nanocrystals indicated by arrows do not have any zone axes.

References and Notes

1. J. C. Meyer, C. O. Girit, M. F. Crommie, A. Zettl, Imaging and dynamics of light atoms and molecules on graphene. *Nature* **454**, 319 (2008). doi:10.1038/nature07094 Medline

2. C.-Y. Wen *et al*., Formation of compositionally abrupt axial heterojunctions in silicon-germanium nanowires. *Science* **326**, 1247 (2009). doi:10.1126/science.1178606 Medline

3. V. Radmilovic *et al*., Highly monodisperse core-shell particles created by solid-state reactions. *Nat. Mater.* **10**, 710 (2011). doi:10.1038/nmat3077 Medline

4. A. H. Zewail, Four-dimensional electron microscopy. *Science* **328**, 187 (2010). doi:10.1126/science.1166135

5. N. de Jonge, F. M. Ross, Electron microscopy of specimens in liquid. *Nat. Nanotechnol.* **6**, 695 (2011). doi:10.1038/nnano.2011.161 Medline

6. M. J. Williamson, R. M. Tromp, P. M. Vereecken, R. Hull, F. M. Ross, Dynamic microscopy of nanoscale cluster growth at the solid-liquid interface. *Nat. Mater.* **2**, 532 (2003). doi:10.1038/nmat944 Medline

7. H. Zheng *et al*., Observation of single colloidal platinum nanocrystal growth trajectories. *Science* **324**, 1309 (2009). doi:10.1126/science.1172104 Medline

8. J. E. Evans, K. L. Jungjohann, N. D. Browning, I. Arslan, Controlled growth of nanoparticles from solution with in situ liquid transmission electron microscopy. *Nano Lett.* **11**, 2809 (2011). doi:10.1021/nl201166k Medline

9. K. S. Novoselov *et al*., Two-dimensional atomic crystals. *Proc. Natl. Acad. Sci. U.S.A.* **102**, 10451 (2005). doi:10.1073/pnas.0502848102 Medline

10. X. Li *et al*., Highly conducting graphene sheets and Langmuir-Blodgett films. *Nat. Nanotechnol.* **3**, 538 (2008). doi:10.1038/nnano.2008.210 Medline

11. J. N. Coleman *et al*., Two-dimensional nanosheets produced by liquid exfoliation of layered materials. *Science* **331**, 568 (2011). doi:10.1126/science.1194975 Medline

12. Z. Lee *et al*., Direct imaging of soft-hard interfaces enabled by graphene. *Nano Lett.* **9**, 3365 (2009). doi:10.1021/nl901664k Medline

13. A. Kolmakov *et al*., Graphene oxide windows for in situ environmental cell photoelectron spectroscopy. *Nat. Nanotechnol.* **6**, 651 (2011). doi:10.1038/nnano.2011.130 Medline

14. Y. A. Wu *et al*., Utilizing boron nitride sheets as thin supports for high resolution imaging of nanocrystals. *Nanotechnology* **22**, 195603 (2011). doi:10.1088/0957-4484/22/19/195603 Medline

15. J. C. Meyer, C. O. Girit, M. F. Crommie, A. Zettl, Hydrocarbon lithography on graphene membranes. *Appl. Phys. Lett.* **92**, 123110 (2008). doi:10.1063/1.2901147

16. R. Erni *et al*., Stability and dynamics of small molecules trapped on graphene. *Phys. Rev. B* **82**, 165443 (2010). doi:10.1103/PhysRevB.82.165443

17. R. R. Nair *et al*., Graphene as a transparent conductive support for studying biological molecules by transmission electron microscopy. *Appl. Phys. Lett.* **97**, 153102 (2010). doi:10.1063/1.3492845

18. J. M. Yuk *et al*., Graphene veils and sandwiches. *Nano Lett.* **11**, 3290 (2011). doi:10.1021/nl201647p Medline

19. K. Xu, P. Cao, J. R. Heath, Graphene visualizes the first water adlayers on mica at ambient conditions. *Science* **329**, 1188 (2010). doi:10.1126/science.1192907 Medline

20. X. Li *et al*., Large-area synthesis of high-quality and uniform graphene films on copper foils. *Science* **324**, 1312 (2009). doi:10.1126/science.1171245 Medline

21. W. Regan *et al*., A direct transfer of layer-area graphene. *Appl. Phys. Lett.* **96**, 113102 (2010). doi:10.1063/1.3337091

22. X. Xie *et al*., Controlled fabrication of high-quality carbon nanoscrolls from monolayer graphene. *Nano Lett.* **9**, 2565 (2009). doi:10.1021/nl900677y Medline

23. S. P. Koenig, N. G. Boddeti, M. L. Dunn, J. S. Bunch, Ultrastrong adhesion of graphene membranes. *Nat. Nanotechnol.* **6**, 543 (2011). doi:10.1038/nnano.2011.123 Medline

24. J. C. Meyer *et al*., The structure of suspended graphene sheets. *Nature* **446**, 60 (2007). doi:10.1038/nature05545 Medline

25. E. A. Stach, Real-time observations with electron microscopy. *Mater. Today* **11**, 50 (2008). doi:10.1016/S1369-7021(09)70007-0

26. H. Zheng, S. A. Claridge, A. M. Minor, A. P. Alivisatos, U. Dahmen, Nanocrystal diffusion in a liquid thin film observed by in situ transmission electron microscopy. *Nano Lett.* **9**, 2460 (2009). doi:10.1021/nl9012369 Medline

27. X. Lu, M. Rycenga, S. E. Skrabalak, B. Wiley, Y. Xia, Chemical synthesis of novel plasmonic nanoparticles. *Annu. Rev. Phys. Chem.* **60**, 167 (2009). doi:10.1146/annurev.physchem.040808.090434 Medline

28. K. J. M. Bishop, C. E. Wilmer, S. Soh, B. A. Grzybowski, Nanoscale forces and their uses in self-assembly. *Small* **5**, 1600 (2009). doi:10.1002/smll.200900358 Medline

29. X. Lu, M. S. Yavuz, H.-Y. Tuan, B. A. Korgel, Y. Xia, Ultrathin gold nanowires can be obtained by reducing polymeric strands of oleylamine-AuCl complexes formed via aurophilic interaction. *J. Am. Chem. Soc.* **130**, 8900 (2008). doi:10.1021/ja803343m Medline

30. P. Schapotschnikow, R. Pool, T. J. H. Vlugt, Molecular simulations of interacting nanocrystals. *Nano Lett.* **8**, 2930 (2008). doi:10.1021/nl8017862 Medline

31. Z. Z. Fang, H. Wang, Densification and grain growth during sintering of nanosized particles. *Int. Mater. Rev.* **53**, 326 (2008). doi:10.1179/174328008X353538

32. A full description of the TEAM project and achievements from this project is available at http://ncem.lbl.gov/TEAM-project/index.html.